Electronic Supplementary Material (ESI) for Chemical Science.

Bonding heterogeneity and lone pair induced anharmonicity resulted in ultralow thermal conductivity and promising thermoelectric properties in *n*-type $AgPbBiSe_3$†

Moinak Dutta,[a] Koushik Pal,[b] Umesh V. Waghmare[b,] and Kanishka Biswas[a,] *

[a]*New Chemistry Unit, Jawaharlal Nehru Centre for Advanced Scientific Research (JNCASR), Jakkur P.O., Bangalore 560064, India*

[b]*Theoretical Sciences Unit, Jawaharlal Nehru Centre for Advanced Scientific Research (JNCASR), Jakkur P.O., Bangalore 560064, India.*

**E-mail: kanishka@jncasr.ac.in*

METHOD

Pair Distribution Function (PDF): For performing X-ray PDF, the samples were finely ground using agate mortar pestle and the powder crystals were then filled in a capillary having diameter of 0.6 mm and is sealed on ends using adhesive. The capillaries then mounted on an instrument holder which is placed right in between the beam source and the image plate. Cryostream was used for the temperature dependent measurement within the range (100 K – 400 K). The Perkin Elmer detector was placed at 230 mm from the sample and data sets were obtained at regular interval of 50 K. A dark measurement was performed prior to every data set, and to obtain the background data sets from empty capillary was taken after each sample. Lanthanum Hexaboride (LaB_6) was used as a standard for calibration purposes in our experiment. The beam spot size had a dimension of 0.5 x 0.5 mm^2 and a fixed energy of 59.83 keV was used.

Processing and normalization of data provided us with G(r), which gives the probability of finding nearest neighbor atoms at a distance r in the material. G(r) is obtained via Fourier transformation of scattering structure function F(Q), using the formula[S1]

$$G(r) = \frac{2}{\pi}\int_{Q_{min}}^{\infty} F(Q) sinQrdQ$$

Where Q is the momentum transfer of the scattering particle. F(Q) is related to structure function S(Q) which is attained from proper correction of scattering data via the relation F(Q) = Q[S(Q)-1].

Modelling of the PDF data was performed using PDFgui[S2] software. All the datasets from 100 K – 400 K were initially modeled using a rock-salt cubic model. The refinement parameters were the lattice parameter, and the ADP values. To minimize the correlation among the ADPs, first ADPs of all the cations (i.e., Ag/Pb/Bi) on the same crystallographic sites were taken same

and are refined. It was then followed by individual refinement of ADPs of the distinct atoms. The first peak of the G (r) vs r plot represents the nearest atom - atom distance, similarly the second peak corresponds to second nearest atom distances (i.e., cation - cation or anion - anion distance) and so on (see Figure S1 below).

For investigating into the off-centering of the cations, ADPs obtained from cubic fit were fixed. The r range was taken 2.5 Å to 3.5 Å. The peak here corresponds to the nearest cation to anion distance (i.e., a/2, a corresponds to lattice distance). The parameters refined were lattice

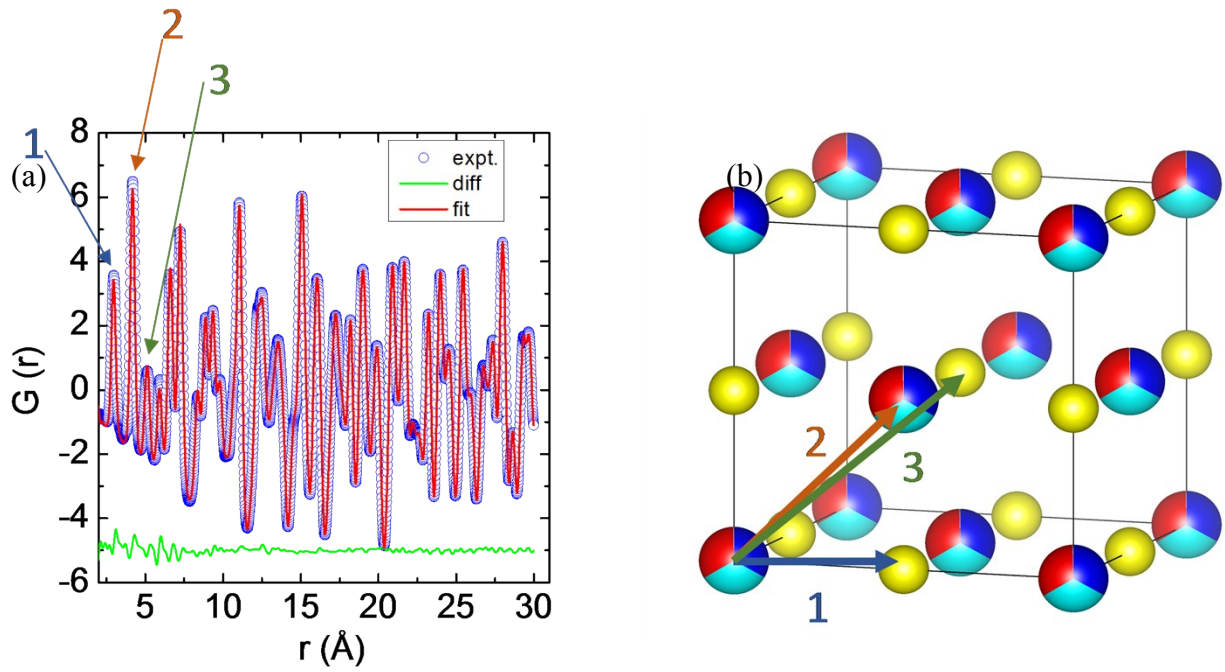

parameters and the cations position in <111> direction.

Fig. S1: G (r) plot in real space which depicts the nearest atom-atom bond distances (part (a)). The peaks marked as 1,2 and 3 corresponds to cation - anion, anion - anion (or cation - cation) and cation-anion distances as shown in part b of the figure.

Determination of κ_{diff}: The minimum lattice thermal conductivity is calculated via diffusion method[S3] using the formula $\kappa_{diff} \approx 0.76 n^{(2/3)} k_B v_s$, where n stands for number density of atoms, k_B is the Boltzmann factor and v_s is the mean velocity of sound derived from experimental heat capacity measurements (1710 m/s). The final value of κ_{diff} is found out to be 0.206 W/mK for undoped AgPbBiSe3 and is used on Fig. 2a and Fig 8e.

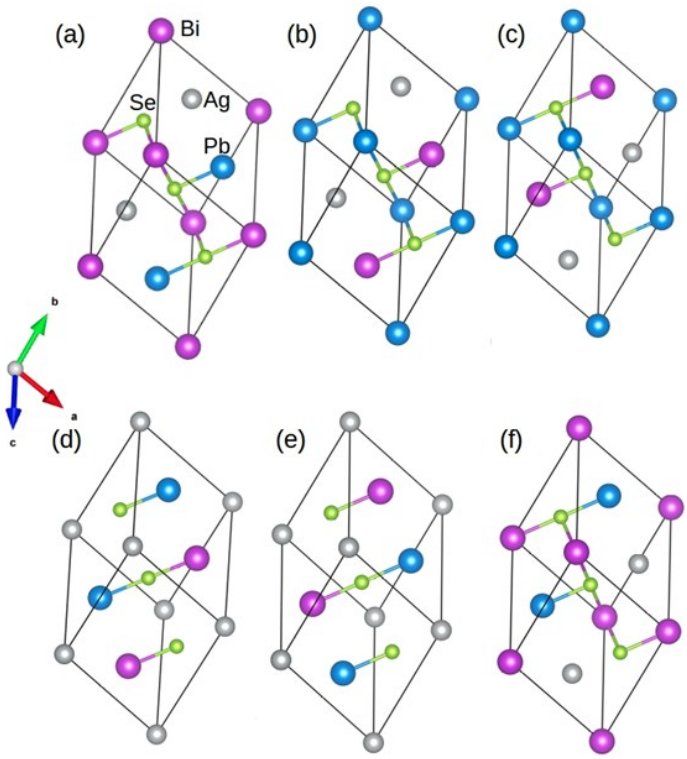

Fig. S2. Six possible configurations of $AgPbBiSe_3$ where the cations are disordered. Our DFT calculations show that all the structures are energetically same. Silver, blue, violet and green spheres represent Ag, Pb, Bi and Se respectively.

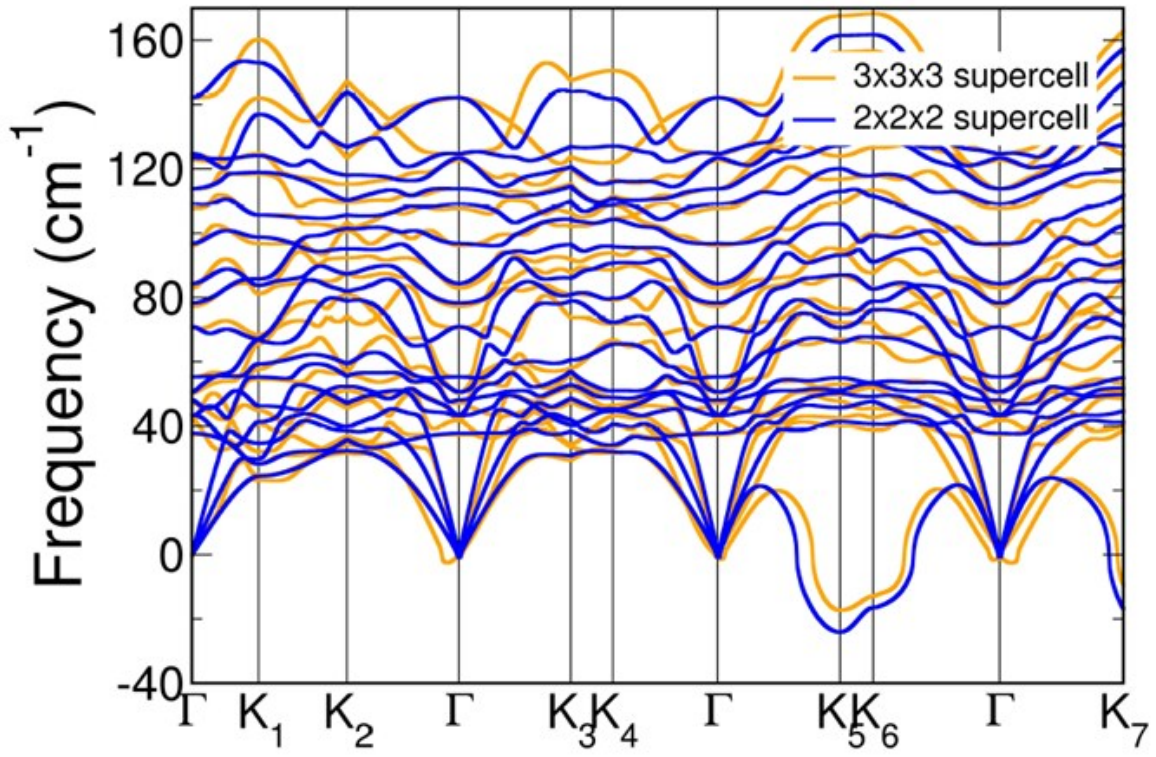

Fig. S3. Phonon dispersion of $AgPbBiSe_3$ calculated with 2x2x2 and 3x3x3 supercell.

To check the convergence of the phonon frequencies with respect to the supercell size, we took 3x3x3 supercell (with 162 atoms) and the same convergence criteria as above with a slightly reduced k-point grid (2x2x2). The changes in the phonon frequencies are not very significant particularly for the acoustic phonon branches. The small negative frequencies around the Gamma point arise probably from the incommensurate nature of the supercell dimension (i.e., 3x3x3) vs k-point grid (2x2x2). Further increase in the supercell size and k-point grid imposes severe computational limitations on the calculations. Hence, for the latter supercell of size 3x3x3, we used 2x2x2 k-point mesh. We believe that increasing the supercell dimension or k-point density will not drastically change the phonon dispersion (Fig. S3, ESI†).

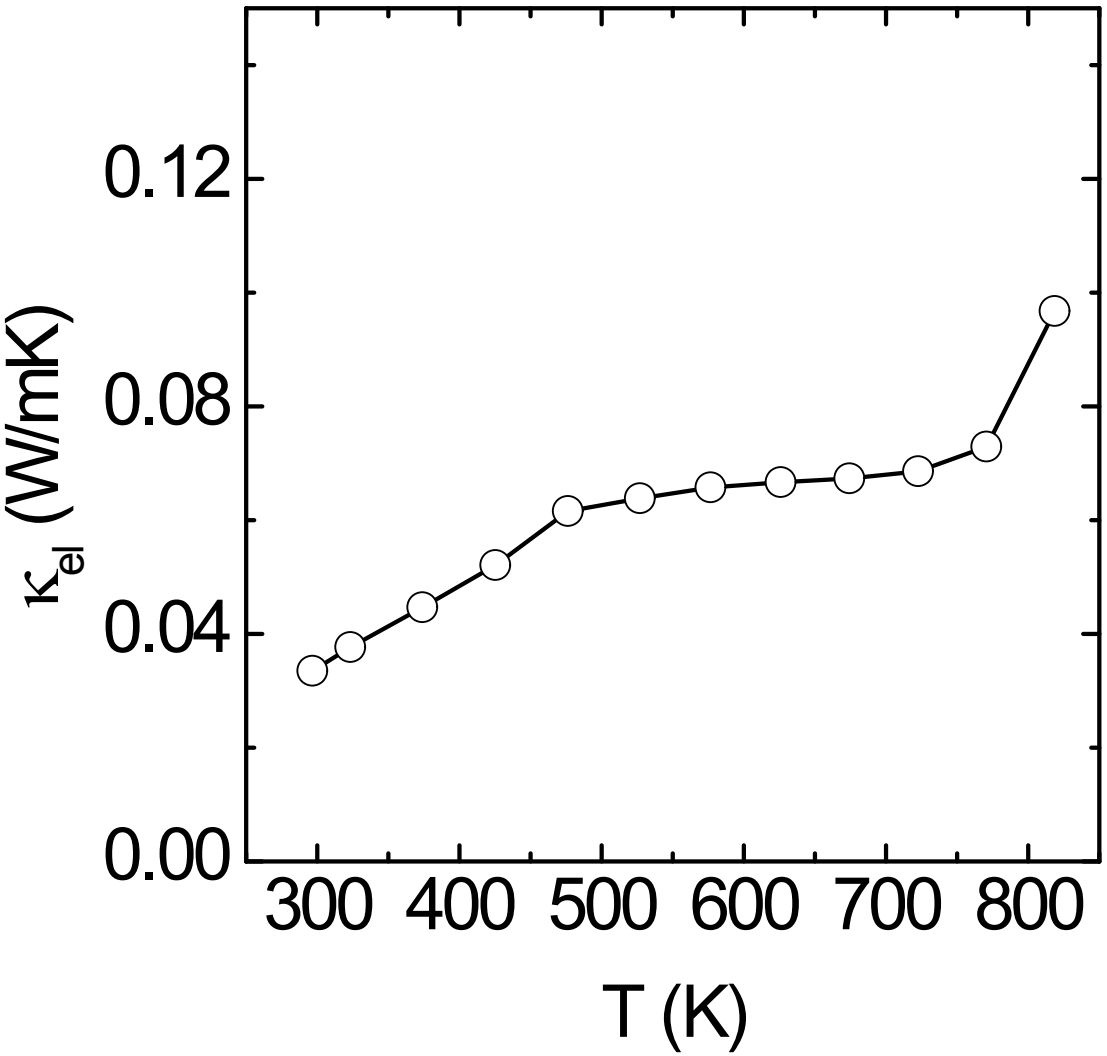

Fig S4. Temperature dependent κ_{el} data for pristine $AgPbBiSe_3$.

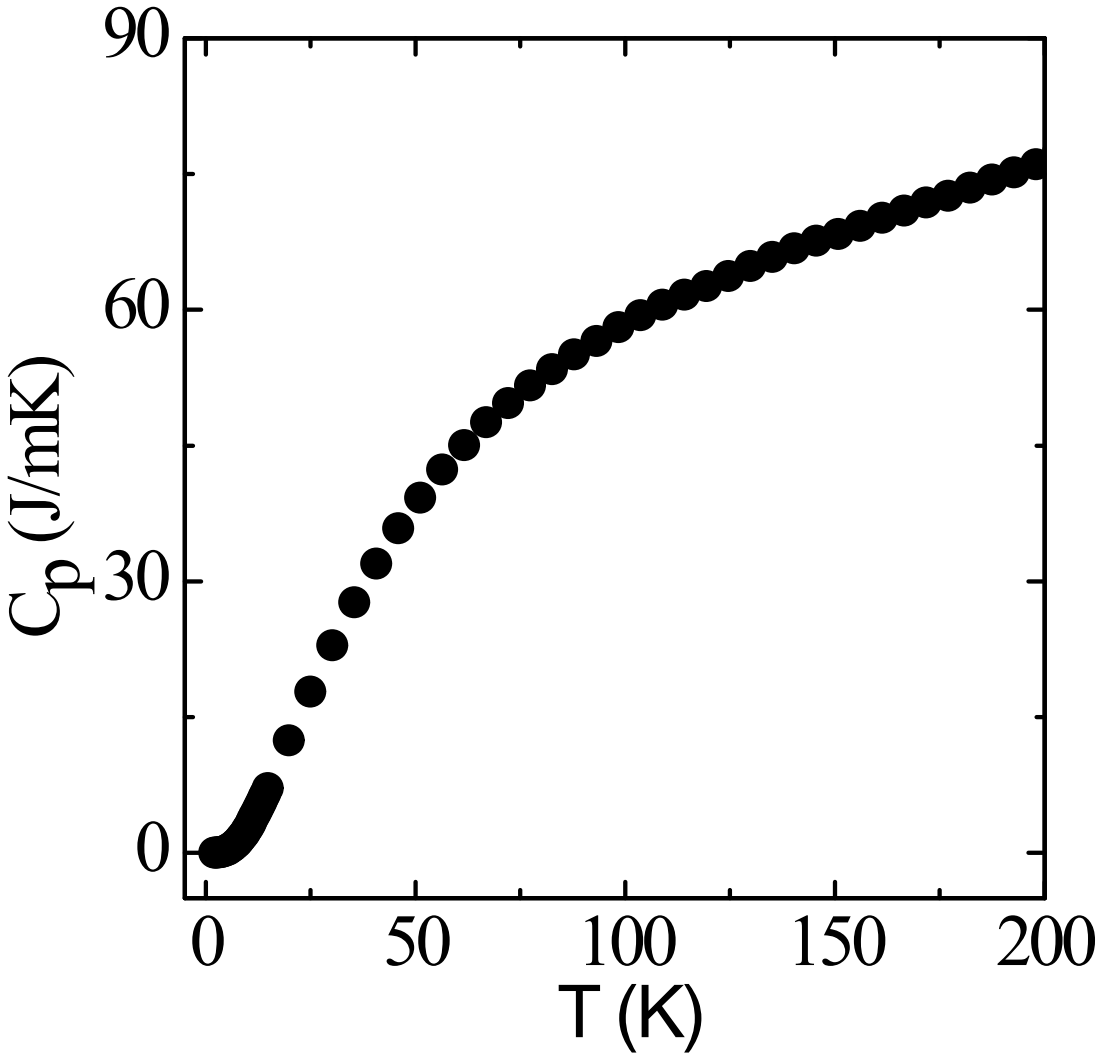

Fig. S5. Temperature dependent heat capacity.

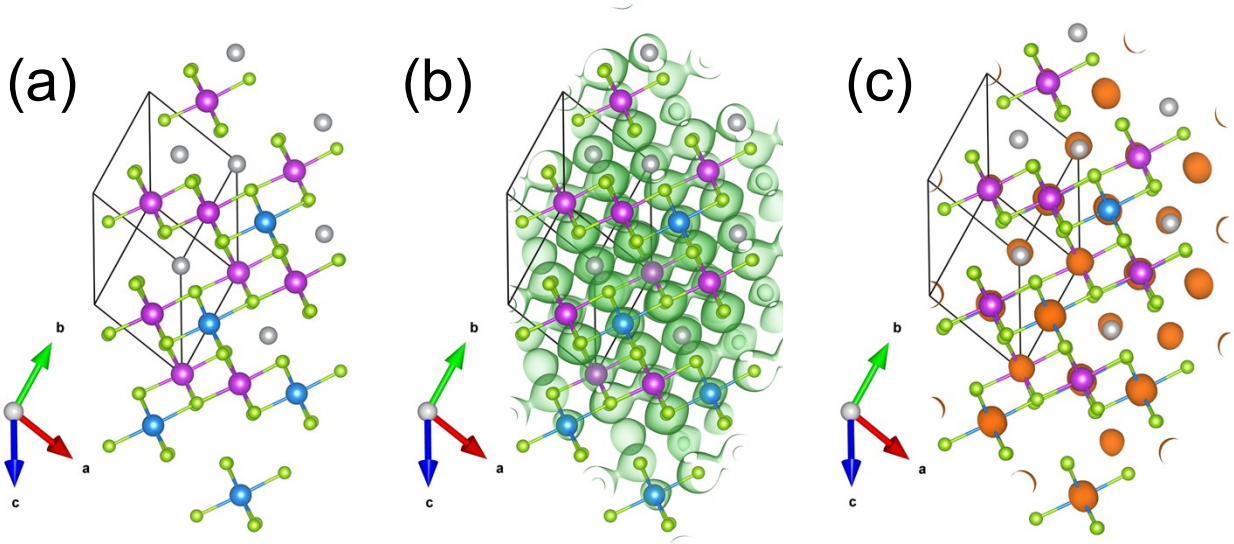

Fig. S6. (a) Supercell containing three primitive fcc unit cells i.e. six atoms (Ag (cyan), Pb (violet), Bi (red) and three Se (green) atoms). (b) Total charge density of $AgPbBiSe_3$ visualized at an iso-value of 0.03 (minimum and maximum iso-values being -0.04 and 1.17, respectively) showing strong overlap of charge densities between Bi and Se atoms, relatively weak overlap between Pb and Se atoms, and almost no overlapping between Ag and Se atoms. (c) Electronic localization function (ELF) visualized at 91 % of the maximum iso-surface value reveals lone pair electrons around Pb and Bi atoms.

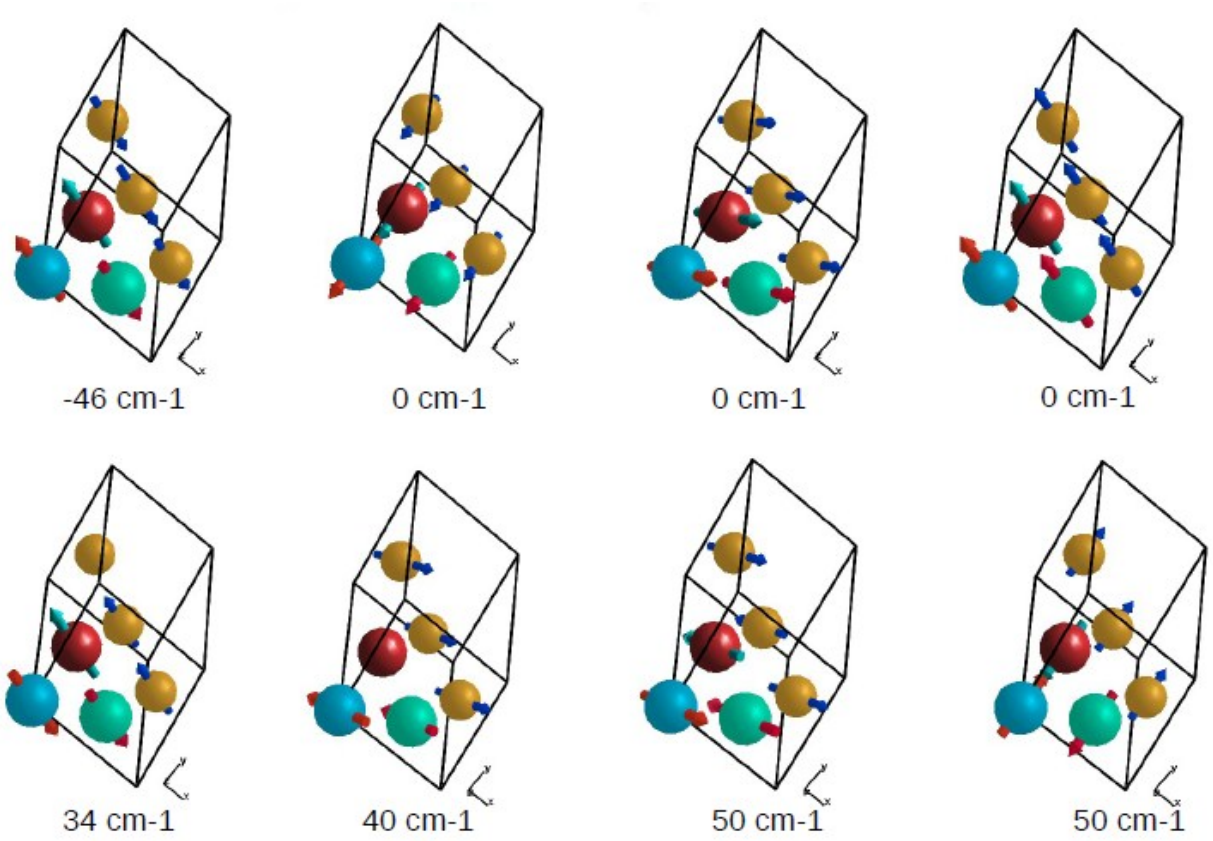

Fig. S7. Visualizations of the atomic vibrations for the phonon modes at Γ point calculated at the optimized lattice constant. Red, Yellow, Cyan and Blue symbolizes Ag, Se, Pb and Bi respectively.

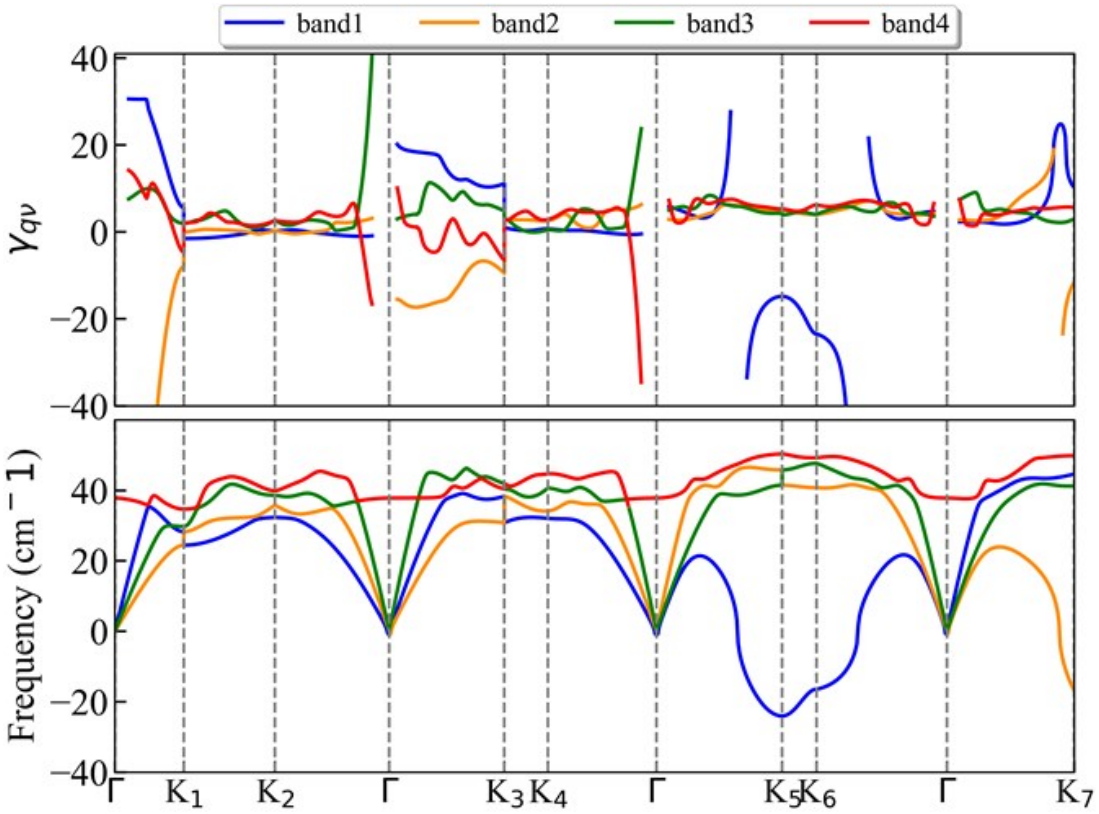

Fig. S8. Mode Gruneisen parameter (γ_{qv}), calculated for the four lowest frequency phonon branches along high symmetric directions in the Brillouin zone. Very high values of γ_{qv} (~ 20) of the acoustic modes indicate the lattice anharmonicity in $AgPbBiSe_3$ induced by the cation disorder in the unit cell as well as by the electrostatic repulsions of their lone pairs.

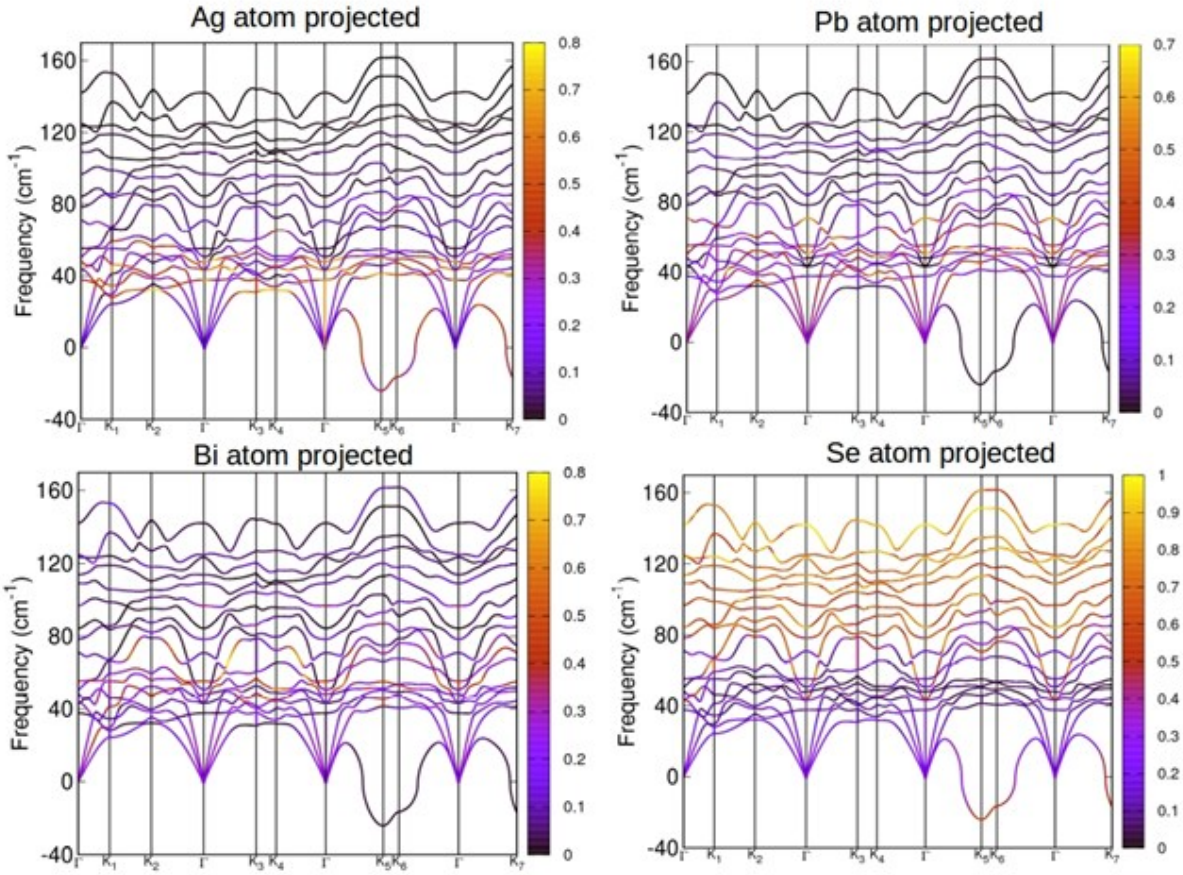

Fig. S9. Atom projected phonon dispersion curves show that while Ag, Pb and Bi atoms primarily contributes to the low frequency (< 50 cm^{-1}) optical phonon branches, Se atom being the lightest element mainly involved in the high frequency (> 50 cm^{-1}) phonon modes in the spectrum.

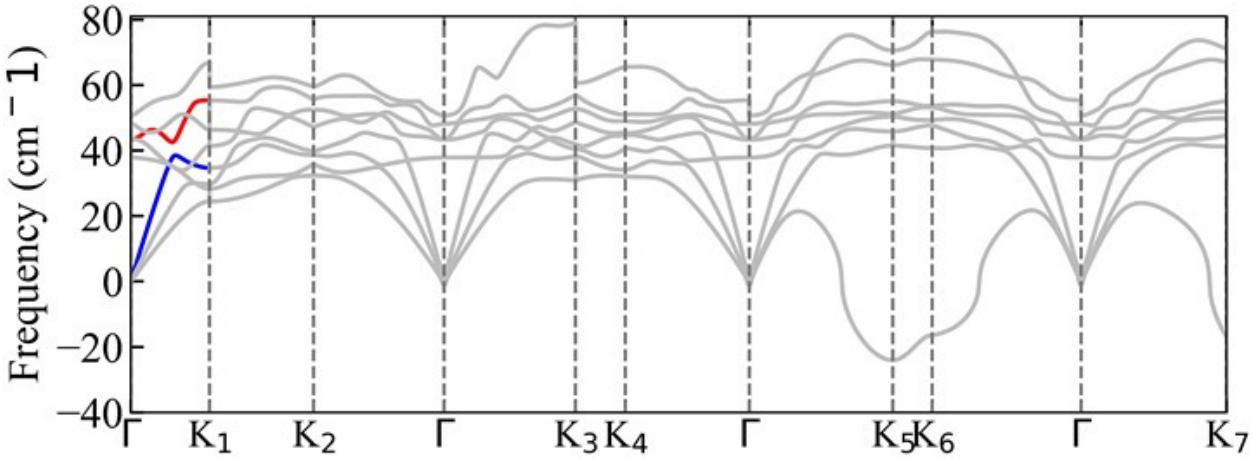

Fig S10. Strong anharmonicity leads to enhanced scattering rate in the lattice, which is also manifested by the avoided crossing between the acoustic (blue line segment) and low frequency optical (red line segment) modes.

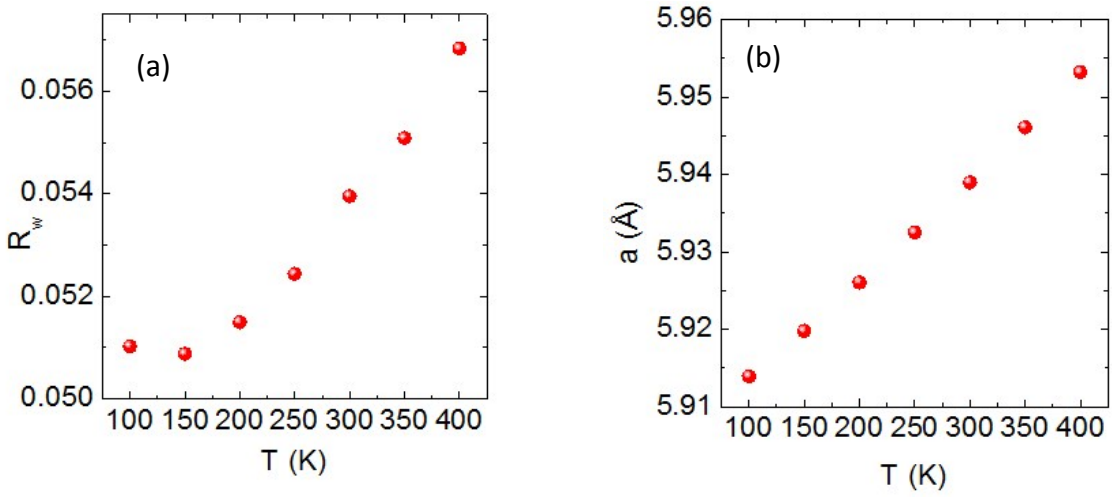

Fig. S11. Temperature dependent (a) R_w and (b) lattice parameter (i.e., a). The values are obtained using refinement of synchrotron X-ray PDF data using undistorted cubic model.

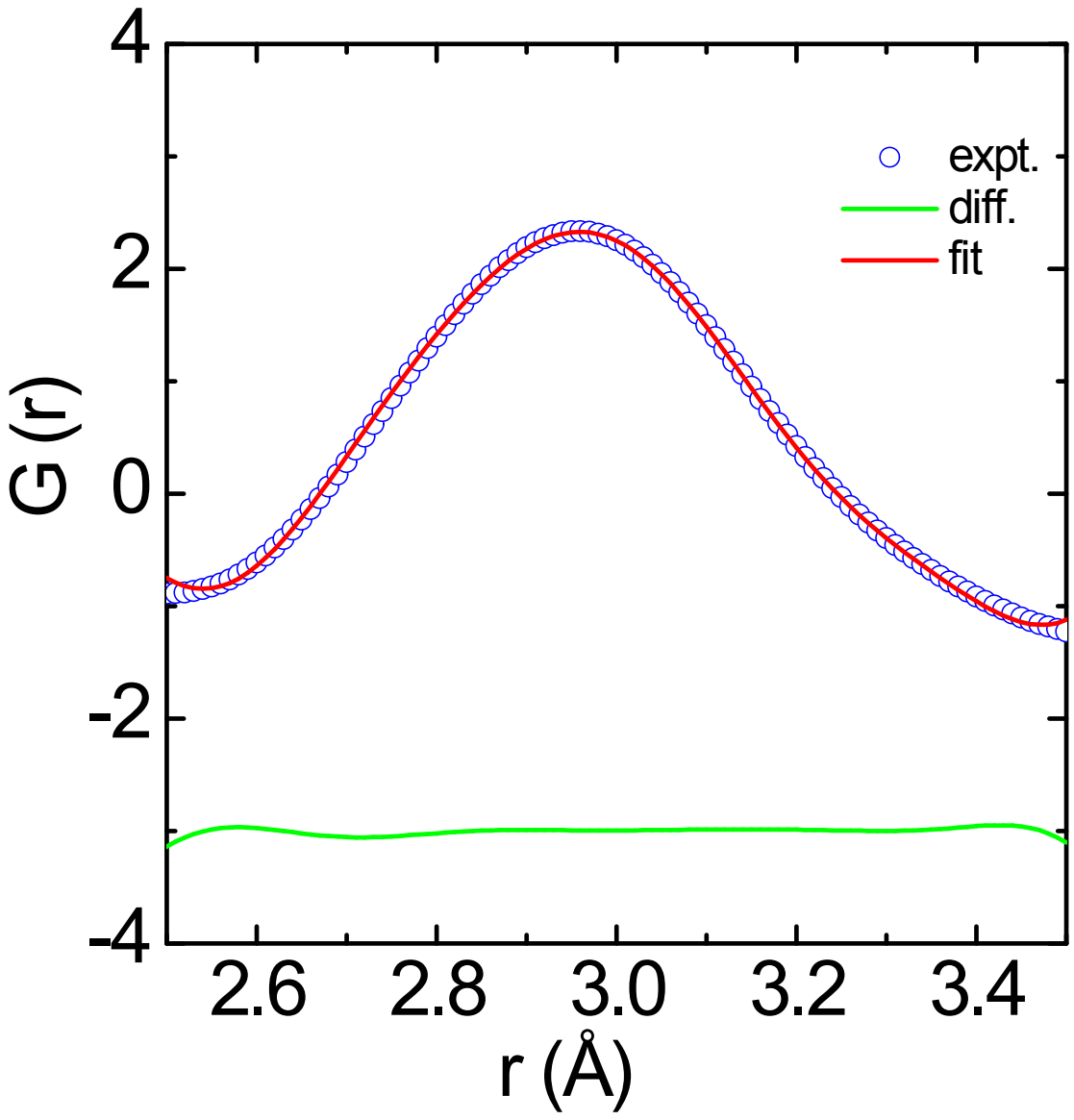

Fig. S12. Local structure fit done at 400 K. The R_w parameter obtained is 2.32%. Fit is obtained by shifting the cations (Ag/Pb/Bi) in the <111> direction.

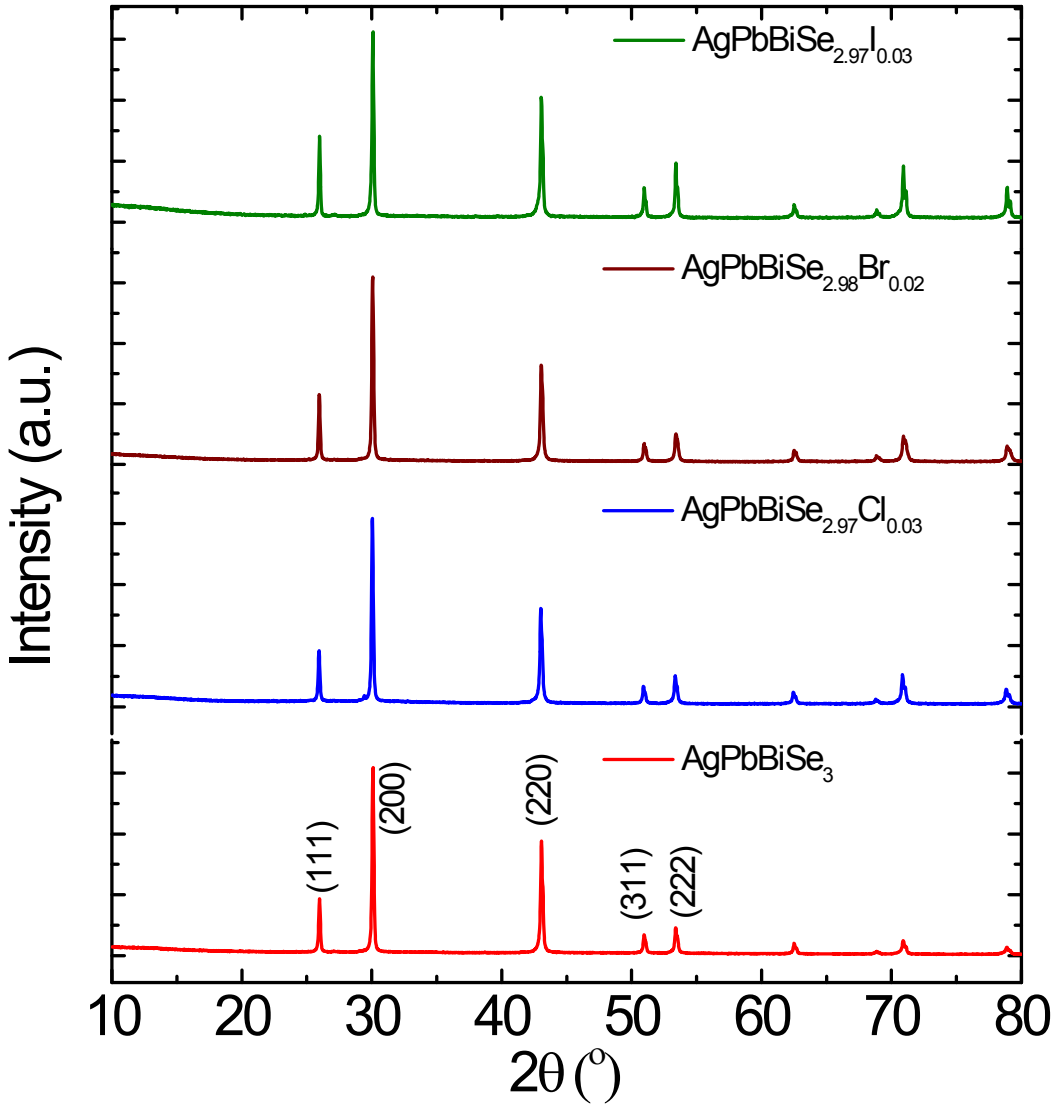

Fig. S13. PXRD pattern of doped halogen compounds. All the compounds pertain rock-salt cubic structure.

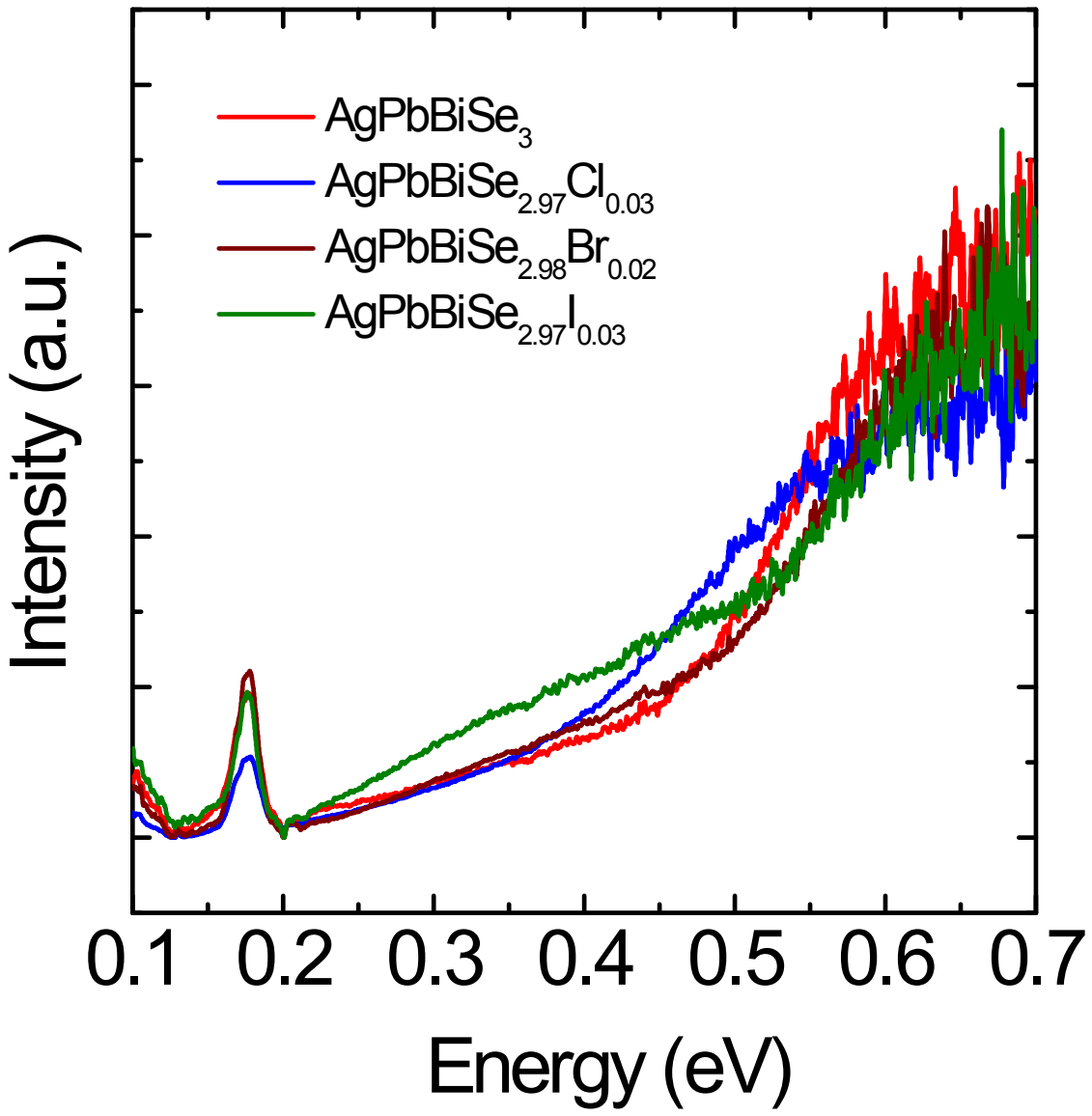

Fig. S14. Band-gap of the pristine and doped $AgPbBiSe_3$.

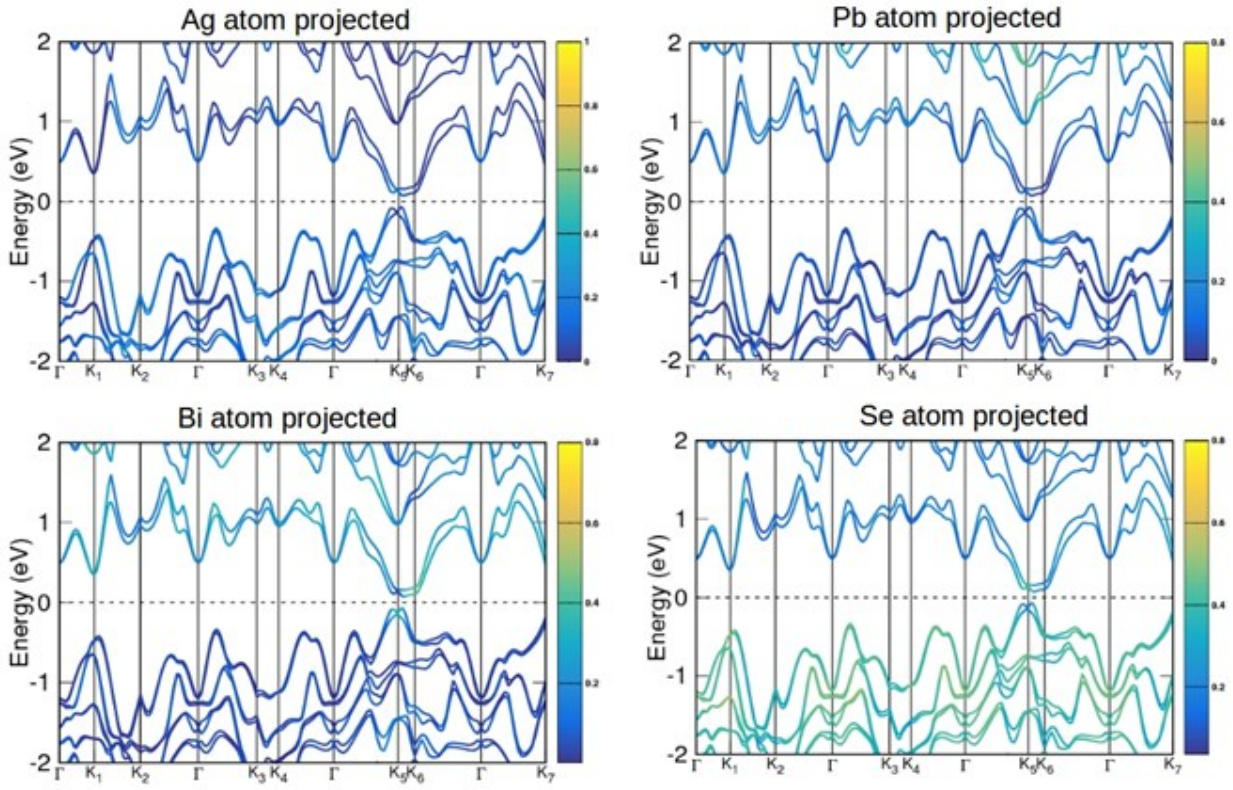

Fig. S15. Atom projected electronic structure of $AgPbBiSe_3$ reveals that while the valence bands just below the Fermi level have highest contributions from the Se atoms, the conduction bands just above the Fermi level have larger contributions coming from the Bi atoms. Ag and Pb atoms have little contributions to the bands in the vicinity of the Fermi level suggesting that they do not actively participate in bonding.

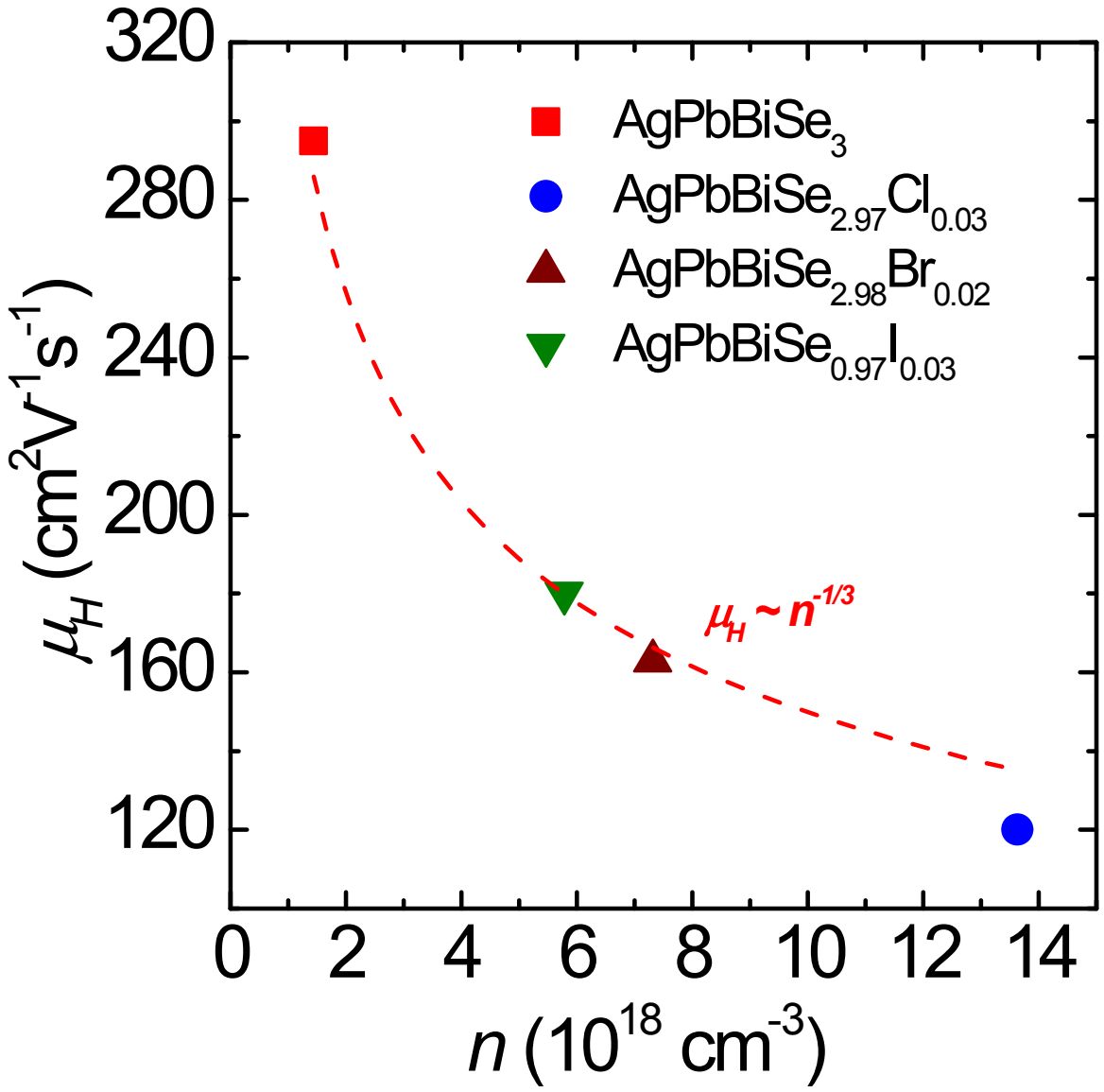

Fig. S16. Mobility (μ_H) vs carrier concentration (n) plot.

Table S1. Parameters obtained after fit in C_p/T vs T^2 plot.

Parameter	values
Υ/ $Jmol^{-1}K^{-2}$	0.01333
β/ $Jmol^{-1}K^{-2}$	1.81949×10^{-4}
Θ_{E1}/K	35.6017
Θ_{E2}/K	74.47509
A_1	4.3697
A_2	21.80491
R^2	0.99974
χ^2	1.31538×10^{-5}

Table S2. Cut off frequencies of different in-plane and out-of-plane directions in $AgPbBiSe_3$

$AgPbBiSe_3$ (ω/ cm^{-1})			
	TA 1	TA 2	LA
Γ-K1	21	27	34
Γ-K3	27	35	42
Γ-K5	19	31	37

Table S3. Temperature dependent ADP values.

T (K)	U_{iso} values (Å^2)			
	Ag	Pb	Bi	Se
100	0.02662	0.01278	0.01277	0.02063
150	0.03042	0.01467	0.01467	0.02321
200	0.03431	0.01688	0.01686	0.02587
250	0.03816	0.01917	0.01931	0.02871
300	0.04191	0.02145	0.0216	0.0316
350	0.04605	0.0239	0.0239	0.03476
400	0.04981	0.02605	0.02606	0.03725

Table S4. Band-gap values for the pristine and doped $AgPbBiSe_3$.

Compound	Band gap (eV)
$AgPbBiSe_3$	0.46
$AgPbBiSe_{2.97}Cl_{0.03}$	0.42
$AgPbBiSe_{2.98}Br_{0.02}$	0.50
$AgPbBiSe_{2.97}I_{0.03}$	0.52

Table S5. Carrier concentration and mobility for the pristine and doped $AgPbBiSe_3$.

Compound	Carrier concentration (cm^{-3}) x 10^{18}	Mobility, μ_H ($cm^2V^{-1}S^{-1}$)
$AgPbBiSe_3$	1.44	295
$AgPbBiSe_{2.97}Cl_{0.03}$	13.63	120
$AgPbBiSe_{2.98}Br_{0.02}$	7.32	163
$AgPbBiSe_{2.97}I_{0.03}$	5.78	180

REFERENCES

S1. P. Th, S. J. L. Billinge, T. Egami and D. Louca, *Z. Kristallogr.* 2003, **218,** 132.
S2. C. L. Farrow, P. Juhas, J. W. Liu, D. Bryndin, E. S. Božin, J. Bloch, P. Th and S. J. L. Billinge, *J. Phys.: Condens. Matter* 2007, **19,** 335219.
S3. M. T. Agne, R. Hanus and G. J. Snyder, *Energy Environ. Sci.* 2018, **11**, 609-616.